Journal of Power Sources 242 (2013) 273–279

Contents lists available at SciVerse ScienceDirect

Journal of Power Sources

journal homepage: www.elsevier.com/locate/jpowsour

The high performance of tungsten carbides/porous bamboo charcoals supported Pt catalysts for methanol electrooxidation

Chun-an Ma*, Chenbin Xu, Meiqin Shi, Guanghui Song, Xiaoling Lang

State Key Laboratory Breeding Base of Green Chemistry Synthesis Technology, School of Chemical Engineering and Materials Science, Zhejiang University of Technology, Hangzhou 310032, Zhejiang, PR China

HIGHLIGHTS

- Bamboo charcoals (BCs) was pre-treated to obtain the high porous structure.
- Three-dimensional (3D) BCs were used as carbon support to synthesize the Pt/WC/BCs electro-catalyst.
- Pt/WC/BCs shows better electrochemical performance compared with Pt/WC/CNTs and Pt/C.
- The enhanced electrochemical performances are related to novel 3D structure of BCs.

GRAPHICAL ABSTRACT

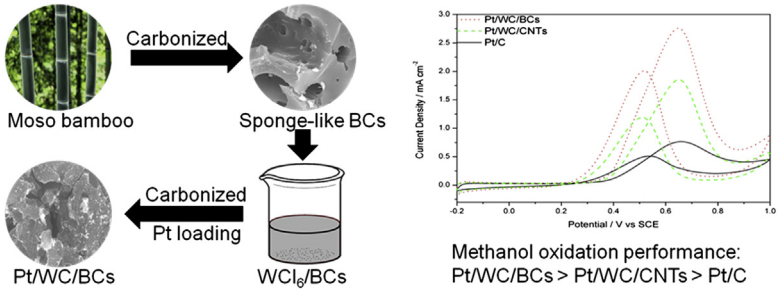

ARTICLE INFO

Article history:
Received 16 January 2013
Received in revised form
18 May 2013
Accepted 19 May 2013
Available online 28 May 2013

Keywords:
Bamboo charcoals (BCs)
Tungsten carbide (WC)
Three-dimensional structure
Methanol oxidation
CO tolerance

ABSTRACT

In this paper, a kind of environmental friendly and cost-effective bamboo charcoal (BC) is used as catalyst support in DMFCs instead of carbon nanotubes (CNTs), which is toxic and expensive. After special treatments, we obtain a sponge-like three-dimensional (3D) BC, which can provide high specific surface area (1264.5 $m^2\ g^{-1}$) and porous matrices. Then, tungsten carbide (WC) and Pt are loaded on the BCs with microwave-assisted technique and 3D structural Pt/WC/BCs electro-catalyst is finally fabricated. Subsequently, the catalyst is characterized by X-ray diffraction (XRD), scanning electron microscopy (SEM) and transmission electron microscopy (TEM). In the further electrochemical investigation, it was found that Pt/WC/BCs catalyst has higher performance (2.76 mA cm^{-2}) and better CO-tolerance for methanol oxidation compared with Pt/WC/CNTs and commercial Pt/C. Herein, we believe that the as-synthesized 3D Pt/WC/BCs catalyst has great promising application in DMFCs.

1. Introduction

Direct methanol fuel cells (DMFCs) are promising power sources for various applications such as vehicles, cell phones or laptops, due to their lower operating temperature and high power density [1,2]. Catalyst is the key factor for high performance in DMFCs and metallic platinum (Pt) is still the most commonly and effectively used anode material [3]. Unfortunately, Pt is a rare and noble metal, in addition, metallic Pt is susceptible to CO-like species during the methanol oxidation even at ppm level, which limits its extensive commercial applications [4–7].

In the searching of solving these problems, tungsten carbide (WC) has been evaluated to be a promising candidate. In electrocatalysis, WC has been selected as the catalyst support for methanol oxidation partly owing to its Pt-like catalytic behavior, partly due to its highly tolerance to carbon monoxide (CO) [8–11]. Our group also proved that Pt/WC (001) is much less susceptible to CO poisoning than Pt by theoretical calculation [12]. Woo and Lee et al

* Corresponding author. Tel./fax: +86 571 88320830.
E-mail address: science@zjut.edu.cn (C.-a. Ma).

0378-7753/$ – see front matter © 2013 Elsevier B.V. All rights reserved.
http://dx.doi.org/10.1016/j.jpowsour.2013.05.083

had synthesized different Pt supported WC (Pt/WC) catalysts as a kind of outstanding CO-tolerance methanol electrooxidation catalysts [13,14].

Although WC can enhance the performance of Pt-based catalysts and protect Pt particles from CO-poisoning, it may not be possible to obtain a WC material of the necessary high surface area due to the relatively high density of WC and high temperature at which carbide synthesis is performed [9]. However, it is important to achieve effective utilization of the available WC catalytic surface, which can help Pt particles receiving more anchor points to produce synergistic effect. Therefore, heterostructural carbon support is introduced to disperse the WC and improve the property of catalyst. Carbon nanotubes (CNTs) are one-dimensional (1D) materials exhibiting excellent properties such as superior mechanical strength, nonlinear optical properties and electrical conductivity, which have been widely used as synergistic host with Pt and WC in DMFCs [15–17]. Liang et al. and Zhao et al. prepared different structure Pt/WC/CNTs catalysts independently, which commonly gave the excellent methanol oxidation performance [18,19]. However, CNTs are expensive and possess potential toxicity [20]. Therefore, three-dimensional (3D) bamboo charcoals (BCs), as a new class of environmental friendly and cost-effective porous carbonaceous materials, have been selected by our group as an ideal substitution of CNTs. The BCs primarily consist of short stacks of graphene sheets, which can form connected porous network after special treatments [21–23]. Bamboo charcoals are now generally used in adsorbing pollutants in air or aqueous solutions. Wang and Zhao et al have proved the excellent capability of bamboo charcoals in absorbing nitrogen-heterocyclic compounds and removing heavy metal ions [24,25]. We believe this structure can also act excellent synergistic effect with Pt and WC through this characteristic porous structure and high specific surface area.

In this work, we pretreated the meso bamboo with phosphoric acid to enlarge original pores and develop new one. After carbonization, these pores can form porous matrixes and shape a sponge-like 3D bamboo charcoals. Subsequently, in vacuum-dried process, the residual moisture in porous is evaporated and form an inner negative pressured condition within bamboo charcoals. We believe that these 3D structure and inner negative pressure effect of bamboo charcoals well give advantage in absorbing and dispersing tungsten source. Finally, we fabricated 3D Pt/WC/BCs and Pt/WC/CNTs catalysts respectively, and the samples were characterized by physical techniques and compared against commercial Pt/C by electrochemical methods.

2. Experimental

2.1. Preparation of BCs

Raw moso bamboo was first impregnated with 85% phosphoric acid for 72 h to enlarge original pores and develop new pores. After centrifugal separation, the resultant bamboo was ground using a ball milling and sieved to the range of 5–30 μm particle size and carbonized in N_2 (100 sccm) at 700 °C for 3 h. Subsequently, semi-finished bamboo charcoals were flushed exhaustively with DI water until the pH value of the filtrate was 7 and vacuum-dried at 60 °C to obtain the final bamboo charcoals samples. After carbonization and vacuum-dried, we ultimately receive a sponge-like and inner negative pressured 3D bamboo charcoals.

2.2. Preparation of Pt/WC/BCs catalyst

The as-synthesized bamboo charcoals were added into the ethanol dissolved with tungsten chloride (WCl_6) at 60 °C. After the ethanol was completely evaporated, the WCl_6/BCs precursor were carbonized in CO atmosphere (100 sccm) at 900 °C for 3 h and defined as WC/BCs.

Synthesizing the Pt/WC/BCs was starting with 5 mM H_2PtCl_6 solution dropping into the WC/BCs precursor. After 2 h ultrasonic dispersion, appropriate amount of ethylene glycol was mixed in the above suspension and transferred into microwave system (Biotage, Initiator EX), where it was rapidly heated to 180 °C for 30 min [26]. Ultimately, the Pt/WC/BCs catalyst was fabricated, and the schematic illustration of formation process is outlined in Scheme 1. In this study, predetermined Pt loading is 10 wt% for all samples.

2.3. Preparation of Pt/WC/CNTs catalyst

We replaced bamboo charcoals with nitrified multi-wall CNTs and used the same methods which were mentioned above to obtain the control Pt/WC/CNTs catalyst. Another comparative sample was the commercial Pt/C catalyst (20% Pt on Vulcan XC-72R, Johnson Matthey Corp.).

2.4. Physical characterization

The catalysts were evaluated by X-ray diffraction (XRD: Thermo ARL X'TRA) patterns, scanning from 15° to 80° at a scan rate of 5° min^{-1} using Cu K_α source. Morphology observations were performed on a scanning electron microscopy (SEM: Hitachi S-4700II), and a transmission electron microscope (TEM: FEI Tecnai G2 F30) equipped with energy-dispersive X-ray fluorescence spectrometer (EDX). Specific surface areas were obtained by nitrogen method at −196 °C using a micromeritics ASAP2020 system and calculated by the Brunauer–Emmet–Teller (BET) method.

2.5. Electrochemical measurements

A glassy carbon (GC) electrode (3 mm in diameter) was used as working electrode, a Pt foil as counter electrode, a saturated calomel electrode (SCE) as reference electrode, and all potentials reported in this paper are corrected to the RHE scale. Before each measurement, 99.99% N_2 gas was bubbled into the electrolyte for 30 min, and the GC electrode was polished with 0.05 μm alumina paste, followed by washing with DI water in an ultrasonic bath. 3 mg catalyst was dispersed ultrasonically in a mixture solution of

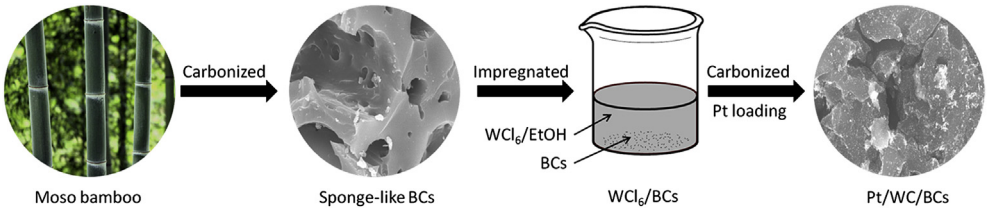

Scheme 1. Illustration of the formation process from moso bamboo to Pt/WC/BCs.

95 μL isopropanol and 5 μL Nafion. Subsequently, 3 μL ink was transferred on the GC electrode. Therefore, we can keep the Pt loading at 0.009 mg on each electrode.

The CO stripping experiments were performed in 0.5 M H_2SO_4 solution. Along with the continuous CO bubbling for 30 min, the anode electrode was controlled at −0.14 V vs SCE electrode for CO adsorption. The solution was then purged with N_2 for 30 min to remove the dissolved CO before stripping tests. All electrochemical measurements were carried out with a computer-controlled electrochemical analyzer (CHI660D CH instruments Inc, Shanghai) in a conventional three-electrode cell.

3. Results and discussion

3.1. Characterization of BCs

The modified bamboo charcoals were characterized by SEM, TEM and BET methods, and the profiles were displayed in Fig. 1 and Fig. 2. From low magnification SEM image (Fig. 1a), we confirm that the BCs bulk size range between 5 and 30 μm, and the inset high magnification SEM image provides direct evidence that the as-synthesized bamboo charcoals have a sponge-like 3D structure. TEM image in Fig. 1b clearly shows that disordered pores are spreading over the surface of bamboo charcoals, which further prove that porous bamboo charcoals had been prepared. For further determining the properties of pores in bamboo charcoals, N_2 adsorption/desorption isotherms and BJH pore-size distribution are plotted in Fig. 2. The extremely high BJH desorption pore area indicates that lots of pores spread over BCs, which is very identical to the observation in TEM image. The characterization results show us a general appearance of bamboo charcoals, and provide the evidences that multi-porous bamboo charcoals have been prepared.

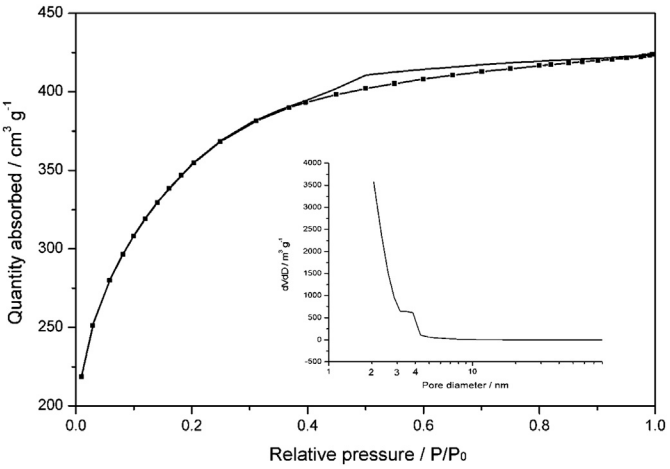

Fig. 2. N_2 adsorption/desorption isotherms of BCs, and the inset corresponds to the pore-size distribution of porous within BCs.

3.2. Characterization of Pt/WC/BCs

3.2.1. XRD measurements

Fig. 3 shows the XRD profiles of Pt/WC/CNTs and Pt/WC/BCs catalysts with 10 % Pt loading. For the Pt/WC/BCs, the strong diffraction peaks at $2\theta = 31.6°$, 35.7°, and 48.6° can be indexed to the (001), (100) and (101) crystal faces of WC (JPCDS No. 25-1047). The characteristics of the face-centered cubic (fcc) Pt crystal are evident as indicated by the orientations along the Pt (111), Pt (200) and Pt (220) directions, at $2\theta = 39.7°$, 46.2° and 67.4°, respectively (JPCDS No. 87-0646). In contrast, the diffraction peaks of Pt/WC/CNTs are similar to Pt/WC/BCs, whereas it is noteworthy that at $2\theta = 26.3°$, the carbon nanotubes diffraction peak (JPCDS No. 01-0640) is much higher than bamboo charcoals. This can be attributed to that amorphous bamboo charcoals partly transformed to graphite pattern and show a weaker graphite carbon peak at $2\theta = 26.3°$. The Pt particle size was calculated by the Scherrer's equation: $D = K\lambda/\beta \cos\theta$, where K is a coefficient (0.9), λ is the wavelength of X-ray used (0.154 nm). Consequently, it can be calculated that the diameter of Pt particle is 4.02 nm (Pt/WC/BCs) and 3.66 nm (Pt/WC/CNTs), respectively.

3.2.2. Morphology observation

Before each morphology observation, Pt/WC/BCs catalyst was grinded in the hope of observing the inner structure. Fig. 4 is the SEM images of Pt/WC/BCs catalyst. First, the typical Pt/WC/BCs image is shown in Fig. 4a, in which, we can discover circuitous connected porous networks and hollow pores structure within bamboo charcoals. Furthermore, in Fig. 4b, we post a close shot of Pt/WC/BCs surface. It is clear that after special managements, the surface of bamboo charcoals has been modified like a kind of multi-

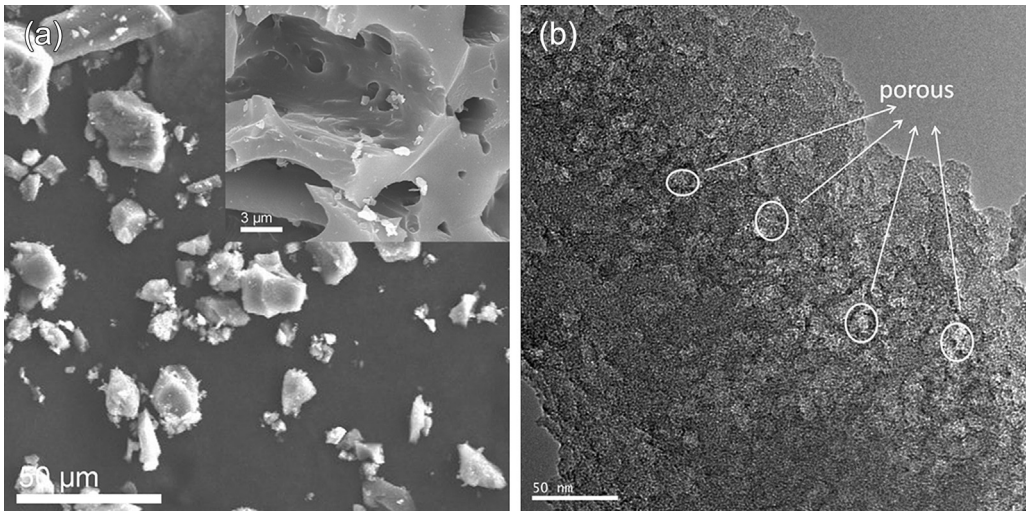

Fig. 1. (a) SEM and (b) TEM images of BCs, and the inset corresponds to the surface details of BCs.

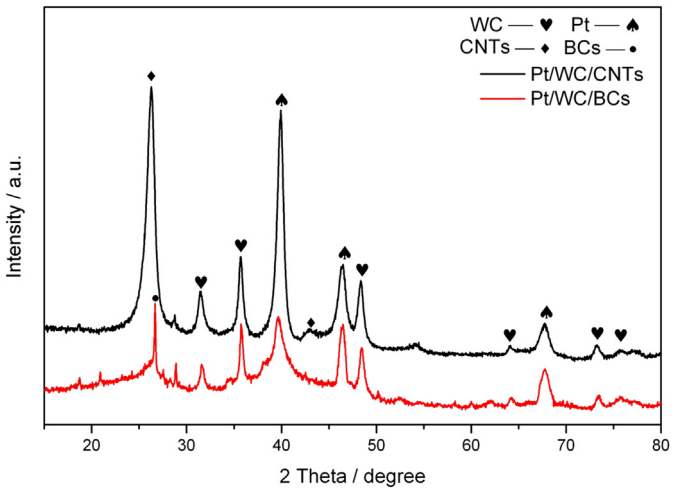

Fig. 3. XRD patterns of Pt/WC/CNTs and Pt/WC/BCs catalysts.

layer cake. Second, an enlarged SEM image of hollow pores is displayed in Fig. 4c, and the details of the pores wall are emerged in Fig. 4d. We can see that Pt/WC particles scattering both on surface and the inner of the bamboo charcoals. We believe it is attributed to the hollow pores structure and inner negative pressured condition within bamboo charcoals, which facilitate absorbing tungsten group. These heterogeneous veins and structure obviously increase the specific surface area, which can be proved by the high S_{BET} value (1264.5 $m^2\ g^{-1}$). These four SEM images provide direct evidences that sponge-like 3D structure Pt/WC/BCs have been successfully prepared.

TEM images of 3D Pt/WC/BCs catalyst are shown in Fig. 5. The evenly distributed Pt and WC particles within bamboo charcoals are shown in Fig. 5a, b, from which, we can even testify that most of WC particles range from 5 to 30 nm. This phenomenon can certify that WC achieve high catalytic surface area and improve its effective utilization, which can help Pt particles receiving more anchor points to produce synergistic effect. Moreover, HRTEM observation (Fig. 5c) reveals that Pt particles are around 4 nm, which is close to the calculated value through XRD. Also, we identify the high crystallinity of catalyst with the interplanar spacing of 0.196 and 0.283 nm, corresponding to the Pt (200) and WC (001), respectively. In our previous work, we have found that Pt/WC (001) is the optimal interfacial structure which is much less susceptible to CO poisoning than Pt [12]. It is also noteworthy that Pt particles are loading on and around WC, which can develop more WC–Pt interaction to increase electrochemical performance and protect Pt particles from CO poisoning. The mapping images together with EDX spectra (Fig. 5d) further indicate that functional Pt and WC particles have successfully loaded within bamboo charcoals and twinned WC–Pt interfaces.

3.3. Electrochemical measurements

To evaluate the resistance to the CO_{ads} poisoning of each catalyst, CO stripping voltammograms were recorded. As being seen clearly in Fig. 6, a negative shift of the well-defined CO stripping peak current can be observed from 0.74 V (Pt/WC/BCs) to 0.77 V (Pt/WC/CNTs) and 0.87 V (Pt/C), indicating the effect of WC in the catalysts on facilitating the removal of CO on Pt active sites. It indicates that Pt/WC/BCs electro-catalyst possess the best capacity to remove the intermediate carbonaceous species quickly and keep the catalytic activity of Pt particles. We believe that the mixing of WC protects the Pt from CO-poisoning. In contrast, after long term CO-poisoning, commercial Pt/C shows the lowest CO-tolerance performance, which may due to Pt particles are lack of WC protection and become inactive during CO-poisoning process.

We can also calculate the electrochemically surface area (ECSA) of Pt particles by the equation [27]: ECSA ($m^2\ g^{-1}$) = 100 Q (μC)/420 (μC cm^{-2}) m (μg), where Q_{CO} is the charge for the CO_{ads} oxidation, m is the metal mass on the electrode, 420 μC cm^{-2} is the assumed charge required for the oxidation of a CO_{ads} monolayer.

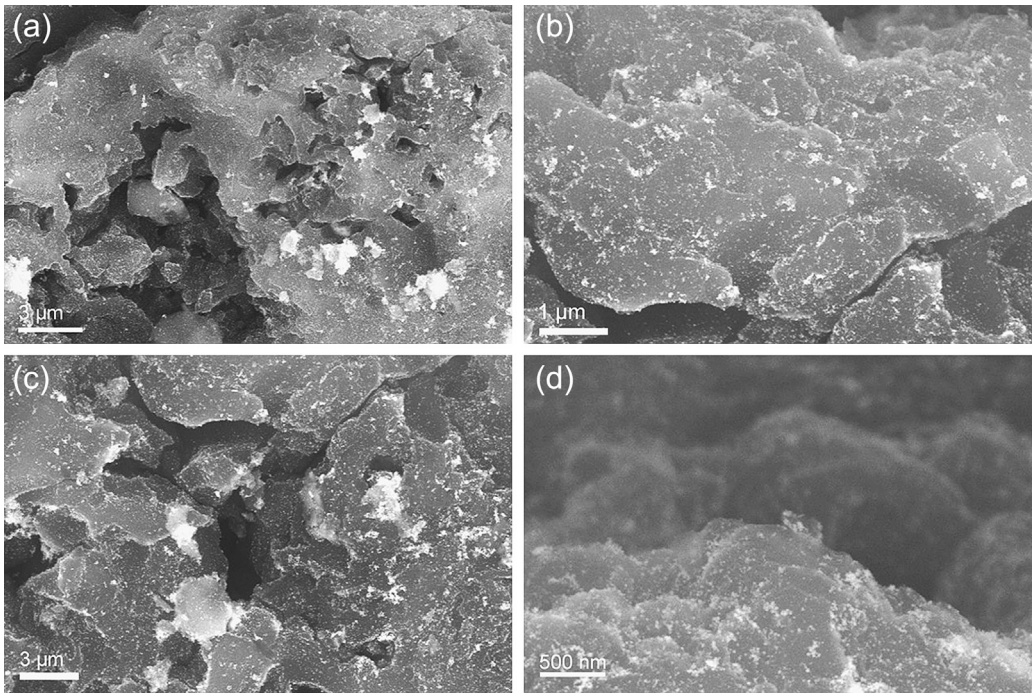

Fig. 4. SEM images of Pt/WC/BCs.

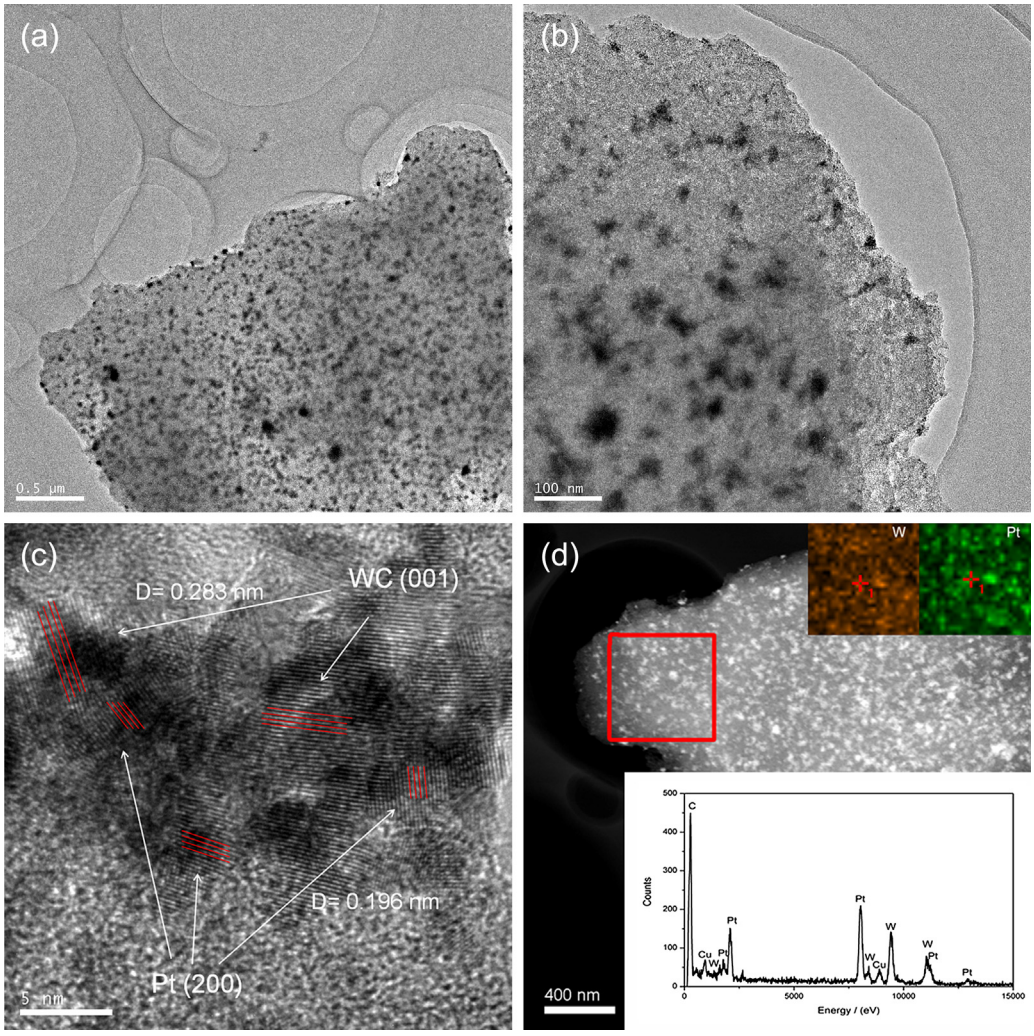

Fig. 5. (a, b) TEM and (c) HRTEM images of Pt/WC/BCs, (d) mapping images of W and Pt, and the inset corresponds to EDX spectra.

Our calculation indicates that the ECSA value of commercial Pt/C is 71.2 $m^2\ g^{-1}$, which is much higher than Pt/WC/BCs (26.1 $m^2\ g^{-1}$) and Pt/WC/CNTs (24.3 $m^2\ g^{-1}$). It is probably due to the fact that Pt particles are smaller on the surfaces of Vulcan XC-72R carbon in the commercial Pt/C. However, smaller Pt particle will not result in a higher catalytic activity, because smaller Pt particles are easier to be oxidized or poisoned and lose its catalytic activity. The research showed that when the Pt particles are about 3–5 nm, it shows the

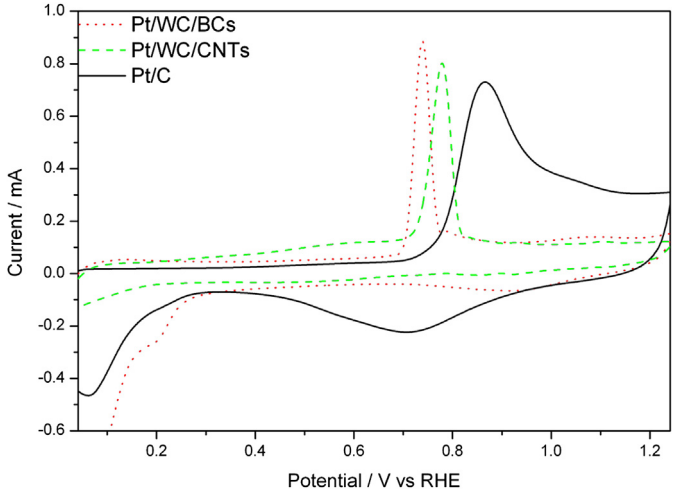

Fig. 6. CO stripping voltammogram curves at room temperature with a scan rate of 50 mV s^{-1} for Pt/WC/BCs, Pt/WC/CNTs and Pt/C.

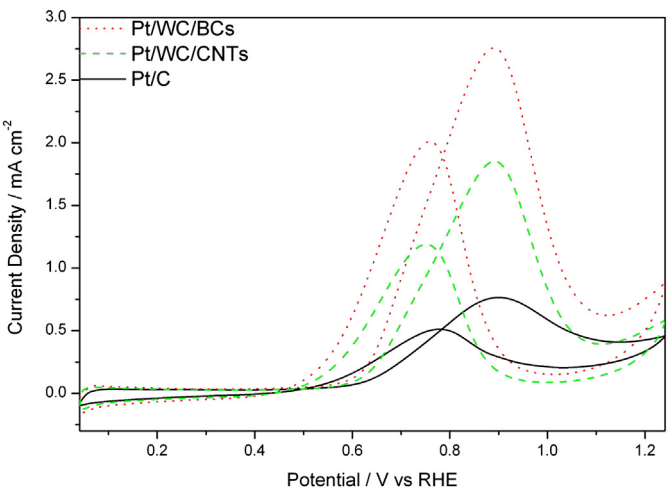

Fig. 7. CV curves of Pt/WC/BCs, Pt/WC/CNTs and Pt/C in 0.5 M H_2SO_4 + 0.5 M CH_3OH solution with a scan rate of 50 mV s^{-1}, $T = 323$ K.

Table 1
Comparison of different parameters among commercial Pt/C, Pt/WC/CNTs and Pt/WC/BCs catalysts.

Samples	Carbon source	S_{BET} ($m^2\ g^{-1}$)[a]	Average Pt size (nm)[b]	ECSA ($m^2\ g^{-1}$)[c]	Current density	
					Per ECSA (mA cm^{-2})	Per mass of Pt (mA mg^{-1} Pt)
Pt/C	C (XC-72R)	254	N/A	71.2	0.74	210
Pt/WC/CNTs	CNTs	117.5	3.66	24.3	1.77	490
Pt/WC/BCs	BCs	1264.5	4.02	26.1	2.76	670

[a] BET surface area (S_{BET}) calculated from the linear part of the BET plot.
[b] The average Pt particle size was calculated by Scherrer's equation.
[c] Electrochemically surface area (ECSA) calculated by the ECSA equation.

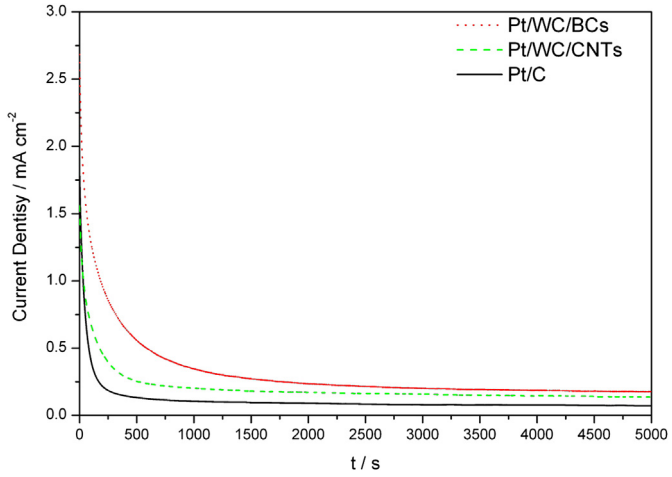

Fig. 8. Chronoamperometry curves at 0.87 V vs RHE in 0.5 M H_2SO_4 + 0.5 M CH_3OH solution with a scan rate of 50 mV s^{-1}, T = 323 K.

best methanol oxidation performance, which is very close to the Pt particles loading in Pt/WC/BCs catalysts [28].

CVs of three electro-catalysts for methanol electrooxidation are measured at 0.5 M H_2SO_4 + 0.5 M CH_3OH solution, which are shown in Fig. 7. Each current density is normalized by the electrochemical active surface area. It shows clearly that the current density of Pt/WC/BCs (2.76 mA cm^{-2}) is much higher than that of the Pt/WC/CNTs (1.77 mA cm^{-2}) and commercial Pt/C (0.74 mA cm^{-2}). Also, we list the current density per mass of Pt value in Table 1. From which, we can discover that the current density of Pt/WC/BCs (670 mA mg^{-1} Pt) is much higher than that of Pt/WC/CNTs (490 mA mg^{-1} Pt) and commercial Pt/C (210 mA mg^{-1} Pt). In both current density analysis, Pt/WC/BCs shows higher electro-catalytic activity than that of its counterparts. We believe that the high methanol oxidation performance is probably caused by the 3D structure BCs and the combination of Pt–WC. The sponge-like 3D structure BCs offer high surface area and obtain the uniform distribution of WC and Pt, which makes full use of WC. Doubtlessly, the high utilization of WC can offer more Pt–WC interfaces to increase the methanol oxidation performance and further enhance the CO tolerance performance of the catalyst.

Fig. 8 shows the chronoamperometric curves for the three types of catalysts at 0.63 V vs SCE in the 0.5 M H_2SO_4 + 0.5 M CH_3OH solution. The oxidation current densities on these three electrodes decrease exponentially with time at the beginning and reach a more or less constant value after several hundred seconds. The final constant currents on the Pt/WC/BCs and Pt/WC/CNTs catalysts are found to be 0.22 and 0.19 mA cm^{-2}, respectively, significantly superior to the Pt/C (0.07 mA cm^{-2}). It is interesting that a slower current decay is observed on the WC supported catalysts, compared with that on the Pt/C catalyst, 18.5% of the initial activity was retained after 500 s of the chronoamperometry on Pt/WC/BCs catalyst, while 14.3% of the initial activity could be maintained on Pt/WC/CNTs catalyst, compared with 8.67% of the initial activity on Pt/C catalyst. This phenomenon confirm a better electro-catalytic stability of the Pt supported WC catalyst, especially with sponge-like 3D structure BCs support, WC and Pt have better environment to play synergistic interaction, leading to both promotion and stabilization of the catalytic activity.

4. Conclusion

In conclusion, we have successfully prepared the Pt/WC/BCs electro-catalyst. Then, the physical characterization results show that Pt/WC/BCs sample has special connected porous networks and sponge-like 3D structure. Subsequently, the electrochemical measurements demonstrate that compared with both Pt/WC/CNTs and commercial Pt/C, Pt/WC/BCs electro-catalyst maintains higher methanol oxidation performance and better CO-tolerance. Herein, we should point out that the as-synthesized 3D Pt/WC/BCs catalyst has great promising application in DMFCs.

Acknowledgment

This work was supported by International Science, Technology Cooperation Program of China (2010DFB63680), Key Project of Natural Science Foundation of Zhejiang Province (Z4100790), Science and Technology Program of Zhejiang Province (2011R09002-08), National Natural Science Foundation of China (21106133).

References

[1] K. Scott, A.K. Shukla, in: R.E. White (Ed.), Modern Aspects of Electrochemistry, Vol. 40, Springer, Berlin, 2007, p. 127.
[2] F. Maillard, E. Peyrelade, Y. Soldo-Olivier, Electrochimica Acta 52 (2007) 1958.
[3] M.S. Wilson, S. Gottesfeld, Journal of Applied Electrochemistry 22 (1992) 1.
[4] D.C. Papageorgopoulos, M. Keijzer, F.A. de Bruijn, Electrochimica Acta 48 (2002) 197.
[5] Z. Sun, X. Wang, Z. Liu, Langmuir 26 (2010) 12383.
[6] H. Igarashi, H. Uchida, M. Suzuki, Y. Sasaki, M. Watanabe, Applied Catalyst A: General 159 (1997) 159.
[7] A. Ersoz, H. Olgun, S. Ozdogan, Journal of Power Sources 154 (2006) 67.
[8] H. Chhina, S. Campbell, O. Kesler, Journal of Power Sources 179 (2008) 50.
[9] N. Ji, T. Zhang, J.G. Chen, Angewandte Chemie 120 (2008) 8638.
[10] C.J. Barnett, G.T. Burstein, A.R.J. Kucernak, K.R. Williams, Electrochimica Acta 42 (1997) 2381.
[11] S. Bodoardo, S. Maja, N. Penazzi, F.E.G. Henn, Electrochimica Acta 42 (1997) 2603.
[12] C. Ma, T. Liu, L. Chen, Applied Surface Science 256 (2010) 7400.
[13] M.K. Jeon, H. Daimon, K.R. Lee, A. Nakahara, S. Woo, Electrochemistry Communications 9 (2007) 2692.
[14] R. Ganesan, D. Ham, J.S. Lee, Electrochemistry Communications 9 (2007) 2576.
[15] G. Li, C. Ma, Electrochimica Acta 52 (2007) 2018.
[16] H. Zengin, W.S. Zhou, J.Y. Jin, Advanced Material 14 (2002) 1480.
[17] P.M. Ajayan, O.Z. Zhou, Topics in Applied Physics 80 (2001) 391.
[18] C. Liang, L. Ding, W. Li, Y. Wang, Energy Environmental Science 3 (2010) 1121.
[19] Z. Zhao, X. Fang, Y. Li, Y. Wang, P. Shen, F. Xie, X. Zhang, Electrochemistry Communications 11 (2009) 2.
[20] M. Kah, X. Zhang, M.T.O. Jonker, T. Hofmann, Environmental Science & Technology 45 (2011) 6011.
[21] P. Liao, S. Yuan, W. Zhang, M. Tong, K. Wang, Journal of Colloid and Interface Science 382 (2012) 74.

[22] Z. Tan, L. Sun, J. Xiang, H. Zeng, Z. Liu, S. Hu, J. Qi, Carbon 50 (2012) 362.
[23] Z. Tan, J. Qiu, H. Zeng, H. Liu, J. Xiang, Fuel 90 (2011) 1471.
[24] Y. Wang, X.J. Wang, M. Liu, X. Wang, Industrial Crops and Products 39 (2012) 81.
[25] X.J. Wang, Y. Wang, J.F. Zhao, Chemical Engineering Journal 174 (2011) 326.
[26] F. Fievet, J.P. Lagier, B. Blin, B. Beaudoin, M. Figlarz, Solid State Ionics 32/33 (1989) 198.
[27] G. Girishkumar, M. Rettker, R. Underhile, D. Binz, K. Vinodgopal, P. Mcginn, Langmuir 21 (2005) 8487.
[28] P.K. Shen, Z. Tian, Electrochimica Acta 49 (2004) 3107.